

# Towards deformation monitoring with UAV-based mobile mapping systems

C. Eling, L. Klingbeil, M. Wieland, H. Kuhlmann  
Institute of Geodesy and Geoinformation,  
The University of Bonn, Nussallee 17, 53115 Bonn, Germany

**Abstract.** In principal unmanned aerial vehicles (UAVs) are well suited for deformation monitoring tasks, when they are equipped with a mapping sensor, such as a laser-scanner or a camera. In order to detect and describe deformations, the UAV-based mapping data has to be registered between two measurement epochs. The most efficient way to realize this registration is the direct georeferencing. This can be combined with a bundle block adjustment in an integrated sensor orientation, when a camera is used as mapping sensor. One crucial point in deformation monitoring is the knowledge about the stochastic model of the acquired data. However, due to the many different calculation steps of the direct georeferencing and the image processing, statements about the quality of UAV-based point clouds are difficult. Therefore, in this paper, an empirical analyses will be presented, which aims to answer the question, if a directly georeferenced UAV-based mapping system is suited to generate data for geodetic monitoring applications. For this purpose, different flight tests have been performed and evaluated.

**Keywords.** UAV, direct georeferencing, GPS/IMU, deformation monitoring

## 1 Introduction

In recent years, micro- and mini-sized unmanned aerial vehicles (UAVs), which have a weight limit of 5 kg and a size limit of 1.5 m (Eissenbeiss (2009)), have been applied more and more in geodetic applications. The reasons for this are that (i) UAVs can acquire detailed object data from different perspectives quickly, (ii) they can get close to objects without any physical contact, (iii) they can overfly inaccessible areas and (iv) they can fly fully or almost fully automatic.

Beside typical surveying applications, UAVs can also be used to realize monitoring measurements such as the monitoring of structural health or the detection of deformations. In many deformation cases the area of interest is not accessible or it even

may involve risks for the operator to stay close to the monitoring area (Baiocchi et al. (2013)). Especially in these cases UAVs can provide a benefit, compared to other monitoring techniques.

One important task for the realization of monitoring applications with UAVs is the registration of data from different epochs. This registration can be realized using ground control points (GCPs), which enable the transformation of the data into a global coordinate system (indirect georeferencing). A second option is given by certain points or areas, which are known to stay constant between the measurement epochs. The third option is the direct georeferencing, which is based on an onboard multi-sensor system. Compared to the first two options, the direct georeferencing offers a number of distinct advantages: It is less time-consuming and can easily be automated. Furthermore, it also allows for operations in inaccessible areas and is not dependent on solid or non moving areas.

Direct georeferencing systems usually include inertial sensors and at least one GPS receiver. Due to a suitable integration of these sensors the position (e.g. X,Y,Z) and the attitude (e.g. roll, pitch, yaw) of the UAV and the mapping sensor can be estimated in real-time onboard of the UAV platform. In recent years, direct georeferencing has extensively been researched and used in airborne applications (Schwarz et al. (1993), Skaloud (1999), Heipke et al. (2002)). First approaches for the realization of a cm accurate positioning of lightweight UAVs can be found in Bláha et al. (2011), Bäumker et al. (2013), Rehak et al. (2014) and Eling et al. (2014). Nowadays also commercial direct georeferencing systems, which are suitable for small UAVs, are available, such as the Ellipse-D system by SBG (SBG (2015)) or the APX-15 UAV by Applanix (Applanix (2015)). We use an in-house developed direct georeferencing unit, which is described in Eling et al. (2014).

As mapping sensor for lightweight mobile mapping systems, such as UAVs, a small laserscanner (Heinz et al. 2015) or a camera (Eling et al. 2015) can be used. In case the system is equipped with a camera, there is the possibility to perform an integrated sensor orientation (ISO) (Colomina and



Molina, 2014), which combines the direct georeferencing with a bundle block adjustment (BA).

The objective of this paper is to investigate, if a UAV-based mapping system, which performs an ISO without the use of GCPs, is suited to generate data for geodetic monitoring applications.

Because the observed differences between two measurement epochs are often in the same size order as the actual measurement accuracy, a crucial point in deformation monitoring applications is the knowledge about the stochastic model of the acquired data.

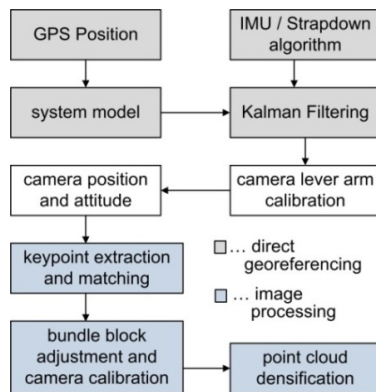


**Fig. 1:** Overview of the calculation steps for the generation of UAV-based mapping data with an ISO.

As shown in Fig. 1 the generation of these data usually includes several calculations steps, such as a GPS positioning, Kalman filtering and BA. Since the stochastic behaviour of some of these steps cannot be modelled completely and the correct propagation of all variances is very difficult, the full covariance matrix of the observed differences is not available so far. Therefore, in this paper, an empirical analysis will be presented, to determine the accuracy of directly georeferenced UAV-based mapping data for deformation analysis. The objective of these investigations is to answer the question, which types and which magnitudes of deformations can be detected with a UAV-based mapping system.

## 2 System design and processing methods

In the following subsections the design of the UAV-based mobile mapping system will be presented. Furthermore, some of the processing methods will be explained.

### 2.1 UAV platform and the direct georeferencing system

The UAV, which has been used in the investigation presented in this paper, is based on the Mikrokopter OktoXL construction kit by HiSystems (Fig. 2). Some modifications of the original setup, such as the realization of a coaxial rotor configuration, enabled the mounting of sensors for the direct georeferencing and the mapping on the UAV platform.

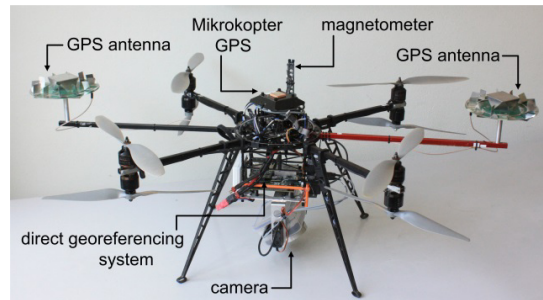


**Fig. 2:** The UAV, equipped with direct georeferencing and mapping sensors.

The direct georeferencing system is mounted in the center of the UAV. It uses the observations of

- two GNSS antennas, which are mounted at the outer end of the UAV arms
- a GNSS reference station, which are received via radio link
- a tactical grade IMU
- a magnetometer, which is placed as far away as possible from the rotors of the UAV

The development of this georeferencing unit is described in details in Eling et al. (2014) and Eling et al. (2015). The key specifications are, that it is small and light-weight (11.0 cm x 10.2 cm x 4.5 cm, 240g) and that it provides high accuracy position and attitude information ( $\sigma_{Pos} < 5$  cm,  $\sigma_{Att} < 0.5$  deg) in real-time. All algorithms, including the GNSS processing and the sensor fusion, are developed in-house, to have the full control over the system and to be able to realize adaptations according to the application.

On top of the UAV a third GNSS antenna can be seen. This belongs to a standard code based GPS receiver, which is used by the UAV flight electronics to enable an automatic way-point flight. Although in theory possible, the position information from the georeferencing unit is not used to control the UAV right now.

The actual mapping sensor is a 16 Megapixel consumer system camera (Lumix GX1) by Pana-

sonic, which is equipped with a 20 mm fixed focal length pancake lens. The total weight of the UAV, including the Lithium Polymer batteries for the power supply, is 3.6 kg. The dimensions of the system are 1.0 m x 0.8 m x 0.35 m and the average flight time is 10-15 min, depending on the wind, the application and the capacity of the batteries.

## 2.2 Camera synchronization and lever arm determination

One crucial point in the development of a directly georeferenced mobile mapping system is precise time synchronization between the georeferencing sensors and the mapping sensors. Unconsidered time delays can lead to significant inaccuracies, depending on the speed of the vehicle.

The pose estimation from the direct georeferencing system is precisely synchronized with the GPS PPS (pulse-per-second). However, our investigations showed that it is neither possible to trigger the Lumix GX1 with a constant or even predictable time offset between the trigger signal and the start time of the exposure, nor there is an official way to get a signal from the camera, which is synchronized with the exposure start time. We therefore modified the camera internally, to extract the signal, which starts the first curtain of the shutter, and to feed it to the georeferencing unit for precise time stamping.

Beside the time synchronization also the lever arm and the boresight angles between the camera and the direct georeferencing system have to be determined. This was done using flight data, where GCPs were used to determine the camera positions and attitudes via an indirect georeferencing. Comparing these indirectly georeferenced camera positions and attitudes to the directly georeferenced camera positions and attitudes led to the lever arm and the boresight angles. More details to the camera time synchronization and the lever arm determination can be found in Eling et al. (2015).

## 2.3 Image processing and point cloud generation

Using the system and the methods described above, it is possible to determine the exterior camera orientation (position and attitude) for every image with an accuracy of a few centimeters. These camera orientations can be used by the photogrammetry software to provide georeferencing information for the generated point cloud (PC). We use a software

called Agisoft PhotoScan to process the images. In a first step all images are aligned using a bundle adjustment procedure. The result is a sparse PC of tie points in a photogrammetric coordinate system. The coordinates of all images are then imported into the software and the tie points are recalculated to be in the GNSS coordinate system. In a third step the PC is densified using multi-view stereo algorithms. The result is a georeferenced and colored PC, which can be used to generate orthophotos or textured meshes in further processing steps. The intrinsic camera parameters are estimated within the bundle adjustment step, separately for each flight.

## 2.4 Point cloud processing

The processing of the PCs has been performed with the open source software Cloudcompare (CloudCompare (2015)). It is used to manipulate and visualize the PCs, generated within this paper, and to calculate differences between PCs. There are several possibilities to calculate the distances between two PCs and to detect changes between clouds of different epochs. One option is the parametrization of the scene using surface models or primitives, such as cylinders or spheres. The change between epochs is then described as a change of these parameters. In this paper we assume that we do not have any previous knowledge about the scene and the expected deformation. Therefore, we do not fit any models to the data. The other options are direct point to point or point to mesh comparisons. We use these methods here and quickly describe them below. There are more advanced methods, such as Multiscale Model to Model Cloud Comparison (M3C2, see Lague (2013), also for a discussion on PC differences), which we do not address here.

In a point to point comparison the nearest neighbor for each point is found in the second PC and the Euclidian distance is calculated. As it can be seen later in the result section, this method has the disadvantage that only absolute and no signed distances can be determined. The distances are also very sensitive to point density differences between the clouds. In a point to mesh comparison a mesh is calculated for one of the clouds (e.g. by interpolating the points with triangles) and then the distance of a point in one cloud to the nearest triangle of the mesh is calculated. This enables the determination of signed distances and avoids artefacts due to density variations.

### 3 Experimental setup

To evaluate the accuracy of the directly georeferenced UAV-based mobile mapping data a test field was established. This test field consists of various objects, which have been placed on an agricultural area. By manipulating these objects between in total four measurement epochs, we simulated various deformations with different strength.

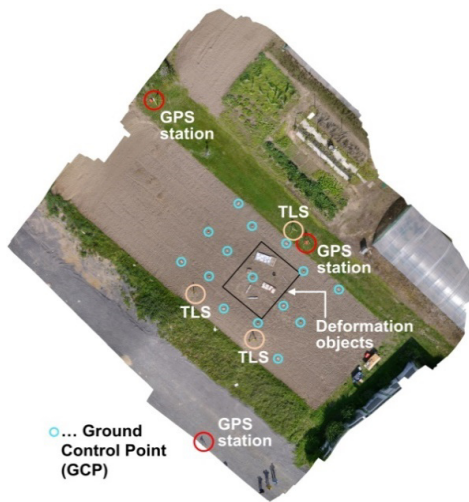


**Fig. 3:** The test field with the deformation object, ground control points (GCPs), some of the GPS stations and the terrestrial laserscanner stations (TLS).

In the geodetic language use, the term deformation comprises both, motions and deformations (Heunecke et al. (2013)). Motions are rigid-body motions (translations and rotations). A subsidence or an uplift of a point or an object belongs to the translations. A tilting of a body around an axis belongs to the rotations. Deformations are changes in the geometry of the object. These can be distortions, bendings or torsions. In the test field at hand not all of the possible motions and deformations were realized, since the effect on the accuracy evaluations is very similar for some of them. The setup of the test field is presented as an orthophoto in Fig. 3 and as a closer image in Fig. 4. In the middle of the area the deformation objects were placed. To be able to analyze the accuracy of the directly georeferenced PC on the ground, fifteen GCPs were distributed uniformly over the field. The coordinates of the GCPs were determined using static GPS measurements at five stations and a tachymeter, leading to mm-accuracies. In order to provide a comparison to an additional measurement tech-

nique, all deformation phases were measured with a terrestrial laserscanner (TLS), which has also been georeferenced using eight of the GCPs.

Altogether, four flights were carried out. The flight height was 20 m, leading to a ground resolution of about 5 mm per pixel. During each flight the area of interest was overflown in multiple stripes with a speed of about 1 m/s, in about five minutes, which leads to ~300 images per flight. Between the first two flights the objects on the ground were not deformed. Between flight 2 and flight 3 only slight motions and deformations were realized. In contrast the motions and deformations between flight 3 and flight 4 were more significant.



**Fig. 4:** The deformation objects in the test field.

In Fig. 4 the test objects are shown. In Table 1 the objects, the type and the approximate magnitude (after flight 2 and flight 3 respectively) of the deformation are listed.

**Table 1:** Description of the deformation objects.

Name	Description	Deformation type
Box 1	Box, 50 x 56 x 27 cm.	Translation along one edge of the box (~5 cm and ~10 cm)
Box 2	Box, 35 x 45 x 15 cm.	Added after flight 2.
Cylinder 1	Lying cylinder, diameter: 14.5 cm, fixed at one side.	Rotation around the horizontal axis upwards (~2 deg and ~5 deg).
Cylinder 2	Lying cylinder, diameter: 14.5 cm, fixed at one side.	Rotation around the vertical axis contra clockwise. (~2 deg and ~5 deg).
Cylinder 3	Standing cylinder, diameter: 31 cm	Translation towards the north (~3 cm and ~10 cm).
Cylinder 4	Lying cylinder, diameter: 7 cm.	No motions or deformations.
Panel	2 x 1 m, 2 cm thick	Rotation around one axis with respect to a second (fixed)

		panel (~1 deg and ~5 deg).
Sheet	Sheet of aluminum, 2 x 1 m, 3 mm thick	Propped up at two edges and in the middle, lowering down the support in the middle (~7 cm and ~10 cm)
Heap	Heap of soil	Vertical deformation (~10 cm and 0 cm)

## 4 Results

The objective of this paper is to evaluate, if directly georeferenced 3D point-clouds from a UAV mapping system can be used to detect small deformations with a magnitude of a few centimeters. Due to space constraints we cannot show the results of all flights and scans, but we will show the main outcome based on a few examples.

### 4.1 Point cloud quality

First, we analyse the general quality of the photogrammetrically derived PC. The quality is mainly dependent on the direct georeferencing, the bundle adjustment and point cloud densification. Fig. 5 shows a detailed view of a resulting PC.



Fig. 5: Detailed view of the photogrammetric PC.

Here the cylinders 1 and 2 can be seen in the foreground. Although the surfaces of the cylinders are straight, significant undulations are visible. These probably result from the image processing step (e.g. search for significant points), which heavily depends on the texture of the objects. Certainly, in case these deviations are different in a second measurement epoch, they have a negative impact on the deformation monitoring. Interestingly, this was not the case in our experiments. A second notable effect is the smoothing of edges, which results from the smoothness assumptions in the point cloud densification process.

To analyze the absolute accuracies of the PC on the ground, the coordinates of the GCPs, which were measured with mm-accuracies using static GPS and a tachymeter, have been compared to the coordinates, resulting from the UAV-based mapping.

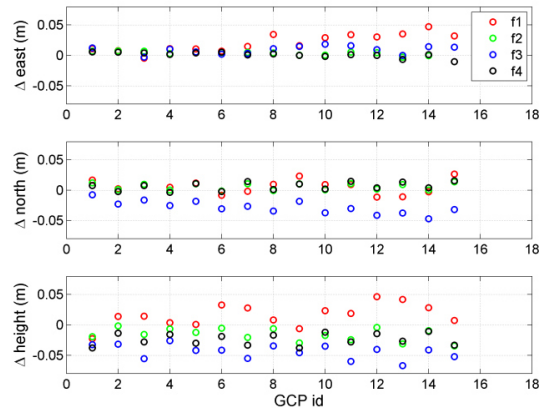


Fig. 6: Differences between the a priori known GCP coordinates and the coordinates measured by the UAV in combination with the photogrammetric processing. f1, f2, f3, f4 denote the four different flights.

The residuals for all fifteen GCPs are shown in Fig. 6. As expected, the height deviations are larger, because both measurement methods are less accurate in their height component (the direct georeferencing due to GPS properties and the photogrammetric processing due to the camera focal length estimation in flat areas). The maximum single point height, east and north deviations are 6.7 cm, 4.7 cm and 4.7 cm in flights 3, 1 and 3 respectively. This shows that the directly georeferenced UAV-based mapping system enables sub-dm accurate single point measurements on the ground. A deeper analysis of these deviations, including the investigation of potential systematic errors is not part of this paper.

### 4.2 Point cloud comparisons

In order to detect deformations, the differences between two measurement epochs have to be determined. Because the result of one measurement epoch is a PC, PC differences have to be calculated.

Fig. 7 shows the point-to-point differences between the directly georeferenced PC of flight 2 and the absolutely georeferenced TLS scan without any motion or deformation of the objects.

A few interesting things can be seen in this figure. First of all, in this example most of the differences

are below 1-2 cm, indicating that the direct georeferencing leads to satisfying results under good GNSS measurement conditions. The many visible small green spots are the footprints of the authors, generated in the loose agrarian soil, while performing the terrestrial laserscan from three viewpoints. In the middle of the test field two red spots are visible. The northern spot results from the short vertical cylinder 3, which could not be reconstructed using the photogrammetric approach. The southern red spot results from a gap in the TLS PC, which was induced by shadowing of the laser. This nicely demonstrates one problem of a point-to-point comparison of PCs: A gap in one cloud leads to high distance values in this area of the other cloud. The inaccuracies of the photogrammetric surface reconstruction of cylinder 1 and 2, as shown in Sec. 4.1, can also be seen in Fig. 7.

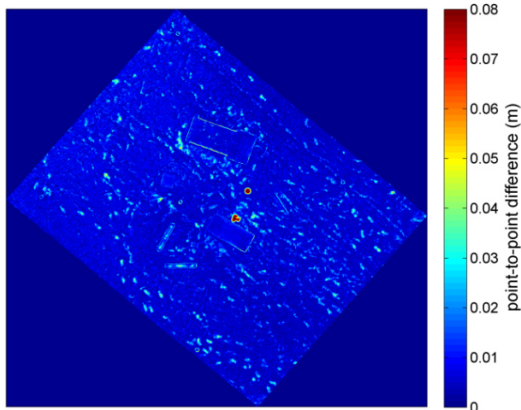


**Fig. 7:** Point to point comparison between the PC of flight 2 and the first TLS scan

For the deformation monitoring with the UAV, the differences of the PCs of the various flights have to be determined. For this, we use point-to-mesh distances. On this account, the ‘reference’ PC (earlier flight) is always triangulated and then differences of the ‘deformed’ PC (later flight) to this mesh are calculated. In this way we are less sensitive to point density variations and we get signed distances as a result.

### 4.3 Accuracy evaluations

As stated in the introduction, not only the differences between two measurement epochs but also the covariance matrix of these differences has to be known, to be able to detect significant deviations, which can be considered as deformations. Since the correct covariance matrix of the points in the UAV-

based PC is unknown, the variances are determined empirically here.

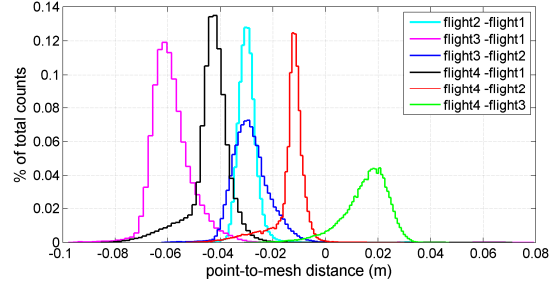


**Fig. 8:** Histograms of the point to mesh differences between PCs of an area of the test field, which is known to be undeformed.

An area of the test field, which is known to be undeformed throughout the whole experiment, has been used to analyze the accuracy of the PC data. Due to the absence of deformations the mean point-to-mesh differences between two flights should ideally be zero with a distribution representing the inner point-cloud accuracies.

In Fig. 8 the histograms of all possible point-to-mesh differences between the different flights are shown for an undeformed area. Assuming a normal distribution for the differences, the standard deviations are in the same order for all six distributions, with a mean of  $\sigma_r \approx 7 \text{ mm}$ . This value is a measure of the precision of the PCs. Due to inaccuracies in the direct georeferencing and in the BA (including the intrinsic camera parameter estimation), the mean values of the resulting distributions are not zero (Fig. 8). Based on these mean values, an empirical standard deviation can be determined to  $\sigma_a \approx 2.6 \text{ cm}$ , which is a measure of the absolute accuracy of the PCs. In the further analysis this empirical standard deviation  $\sigma_a$  is used to detect significant deformations. As confidence level for this deformation detection we use 95 %. Since the sample of six values is very small, not the normal distribution but the student distribution confidence level has to be used. For a two sided test and six degrees of freedom, this value is 2.447. With  $\sigma_a \cdot 2.447 \approx 6.3 \text{ cm}$  the confidence region is:

$$P(-6.3 \text{ cm} < x_d < 6.3 \text{ cm}) = 0.95$$

### 4.4 Detection of deformations

Fig. 9 presents the detected deformations between flight 2 and 3. Red bordered regions visualize deformations with a positive sign and green bordered

regions visualize deformations with a negative sign. Box 2, which was added to the test field in the south (red area), is well detected. Also the bending of the sheet of aluminum can be seen. Some of the footprints are visible and the removal of soil around the heap of soil in the south east of box 2 can also be seen at a few spots. All other smaller deformations are not significant according to the threshold, derived above.

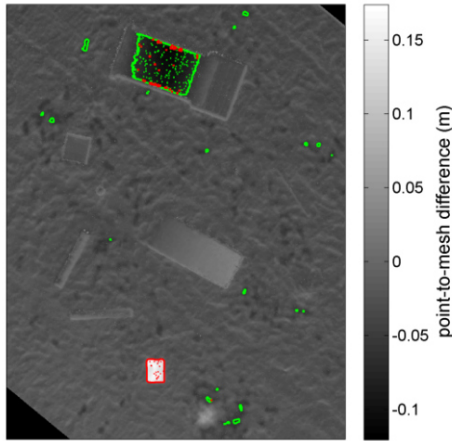


**Fig. 9:** As significant detected deformations in the point to mesh differences between the flights 2 and 3. Green bordered areas are significant negative and red bordered areas are significant positive deformations.

In Fig. 10 the detected deformations between flight 2 and 4 are shown. The deformations between these flights are the maximum deviations available in our experiment. It can be seen that most of the deformations at the sheet of aluminum are visible now. The deformations at the boxes 1 and 2, the panel and cylinder 1 and 2 are also significant. The heap of soil, which was not deformed any further between flight 3 and 4 is now visible as a positive change (the heap itself), while it was a negative change in Fig. 9 (the excavated area around the heap). This may be due to an offset between the two PCs.

Summarizing, this experiment illustrates that the presented directly georeferenced UAV and the ISO are well suited to detect deformations having cm-dm magnitudes and more. However, due to the GSD of  $\sim 5$  mm and an approximate BA matching accuracy of  $\sim 1$  pixel, the inner accuracies of the PCs should be in the order of a few mm, which has been confirmed in section 4.3 ( $\sigma_r \approx 7$  mm). By comparison, the absolute accuracy, which is mainly affected by the direct georeferencing, is one order

worse. To get an idea of what might be possible, if also the absolute accuracy would be better, a fine registration of the two PCs can be done, using the iterative closest point algorithm (ICP).

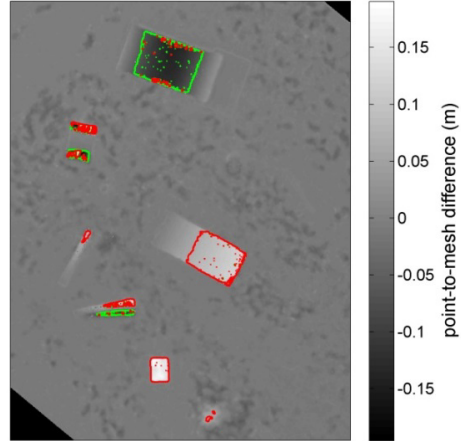


**Fig. 10:** As significant detected deformations in the point to mesh differences between the flights 2 and 4. Green bordered areas are significant negative and red bordered areas are significant positive deformations.

Assuming, that the majority of the area remains unchanged, the systematic offset between the clouds can be removed after registration and only the deformations remain. Due to the smaller standard deviation of  $\sigma_r \approx 7$  mm and the student distribution value of 2.447, the confidence level for deformation detections based on the fine registered PC is:

$$P(-1.8 \text{ cm} < x_d < 1.8 \text{ cm}) = 0.95$$

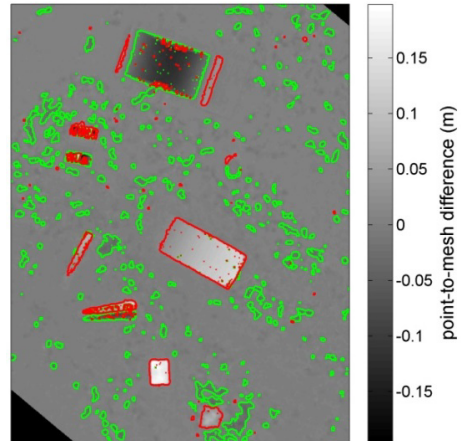


**Fig. 11:** As significant detected deformations in the point to mesh differences between the flights 2 and 4, when the ICP is applied before. Green bordered areas are significant negative and red bordered areas are significant positive deformations.

Fig. 11 shows the differences between the PC from flight 2 and the fine registered PC from flight 4. It can be seen that all deformations are visible now. Even the footsteps on the field are detected as significant deformations. It should be noted that although a georeferencing does not seem to be necessary at all for this last example of analysis, the precise knowledge of the camera positions may significantly improve the BA quality.

## 5 Conclusion

In this paper a UAV-based mobile mapping system was presented, which is equipped with an in-house-developed direct georeferencing system and a camera as mapping sensor. By means of flight tests, it could be shown that this system leads to an efficient way of monitoring deformations. This also applies to inaccessible areas.

Accuracy evaluations revealed that deformations with a magnitude of  $> 6.3$  cm can be detected correctly as significant with this system. In case an additional fine registration via an ICP is applied, remaining systematic errors in the absolute accuracies of the PCs can also be reduced. In this case at least deviations with a magnitude of  $> 1.8$  cm can be detected correctly, when the UAV flies with a height of  $\sim 20$  m above the ground.

Since UAV-based deformation detections rely on the accuracy of PC comparisons, the technique of determining the differences between two PCs is very important. At this point there are still improvements possible in further investigations.

## Acknowledgements

This work was funded by the DFG (Deutsche Forschungsgemeinschaft) under the project number 1505, 'Mapping on Demand'.

## References

- Applanix (2015). APX-15 UAV. <http://www.applanix.com/products/airborne/apx15uav.html>, 09.09.2015.
- Baiocchi, V., D. Dominici, M. Mormile (2013). UAV application in post-seismic environment. In: *Proc of the UAV-g 2013 conference*. International Archives of the Photogrammetry, Remote Sensing and Spatial Information Sciences, Volume XL-1/W2, pp 21-25.
- Bäumker, M., H.-J. Przybilla, A. Zurhorst (2013). Enhancements in UAV flight control and sensor orientation. In: *Proc of the UAV-g conference*. International Archives of the Photogrammetry, Remote Sensing and Spatial Information Sciences, Volume XL-1/W2, pp. 33-38.
- Bláha, M., H. Eisenbeiss, D. Grimm, P. Limpbach (2011). Direct georeferencing of UAVs. In: *Proc of the UAV-g conference*. International Archives of the Photogrammetry, Remote Sensing and Spatial Information Sciences, Volume XXXVIII-1/C22, pp. 131-136.
- CloudCompare (version 2.6.1) [GPL software]. EDF R&D, Telecom ParisTech (2015). Retrieved from <http://www.cloudcompare.org/>.
- Colomina, I., P. Molina (2014). Unmanned aerial systems for photogrammetry and remote sensing: A review. *ISPRS Journal of Photogrammetry and Remote Sensing*, 92,79-97
- Eisenbeiss, H. (2009). UAV Photogrammetry. PhD thesis, ETH Zurich No 18515.
- Eling, C., L. Klingbeil, H. Kuhlmann (2014). Direct georeferencing of micro aerial vehicles - system design, system calibration and first evaluation tests. *PFG - Photogrammetrie, Fernerkundung und Geoinformation* 4, pp. 227-237.
- Eling, C., M. Wieland, C. Hess, L. Klingbeil, H. Kuhlmann (2015). Development and evaluation of a UAV based mapping system for remote sensing and surveying applications. In: *Proc of the UAV-g conference*. International Archives of the Photogrammetry, Remote Sensing and Spatial Information Sciences, Vol. XL-1/W4, pp. 233-239
- Heinz, E., C. Eling, M. Wieland, L. Klingbeil, H. Kuhlmann (2015). Development, Calibration and Evaluation of a Portable and Direct Georeferenced Laser Scanning System for Kinematic 3D Mapping, *Journal of Applied Geodesy* 9(4)
- Heipke, C., K. Jacobsen, H. Wegmann (2002). Integrated sensor orientation - test report and workshop proceedings. In: *OEEPE Official Publication* 43, Frankfurt/Main
- Heunecke, O., H. Kuhlmann, W. Welsch, A. Eichhorn, H. Neuner (2013). *Handbuch Ingenieurgeodäsie - Auswertung geodätischer Überwachungsmessungen*. Wichmann, ISBN 978-3-87907-467-9
- Lague, D., Brodu, N., Leroux, J. (2013). Accurate 3D comparison of complex topography with terrestrial laser scanner: Application to the Rangitikei canyon (NZ), *ISPRS Journal of Photogrammetry and Remote Sensing* 82, pp. 10-26
- Rehak, M. R. Mabillard, J. Skaloud (2014). A micro aerial vehicle with precise position and attitude sensors. *PFG - Photogrammetrie, Fernerkundung und Geoinformation* 4, pp. 239-251.
- SBG (2015): Ellipse-d: Miniature dual GPS INS, <http://www.sbg-systems.com/products/ellipse-d-dual-antenna-gps-inertial-system>, 09.09.2015
- Schwarz, K.-P., M. Chapman, M. Cannon, P. Gong (1993). An integrated INS/GPS approach to the georeferencing of remotely sensed data. *Photogrammetric Engineering & Remote Sensing* 59(11), pp. 1667-1674.
- Skaloud, J. (1999). Optimizing Georeferencing of Airborne Survey Systems by INS/DGPS. PhD thesis, University of Calgary, Canada.